Clays and Clay Minerals, Vol. 58, No. 6, 772–782, 2010.

XAS STUDY OF Fe MINERALOGY IN A CHRONOSEQUENCE OF SOIL CLAYS FORMED IN BASALTIC CINDERS

LESLIE L. BAKER*, DANIEL G. STRAWN, KAREN L. VAUGHAN†, AND PAUL A. MCDANIEL
Soil and Land Resources Division, University of Idaho, Moscow, ID 83844-2339, USA

Abstract—The characterization of poorly crystalline minerals formed by weathering is difficult using conventional techniques. The objective of this study was to use cutting-edge spectroscopic techniques to characterize secondary Fe mineralogy in young soils formed in basaltic cinders in a cool, arid environment. The mineralogy of a chronosequence of soils formed on 2, 6, and 15 thousand year old basaltic cinders at Craters of the Moon National Monument (COM) was examined using synchrotron-based X-ray absorption fine structure (XAFS) spectroscopy in combination with selective extractions. Fe K-edge XAFS is useful for determining speciation in poorly crystalline materials such as young weathering products. Over 86% of Fe in the soil clay fractions was contained in poorly crystalline materials, mostly in the form of ferrihydrite, with the remainder in a poorly crystalline Fe-bearing smectite. The XAFS spectra suggest that ferrihydrite in the 15 ka soil clay is more resistant to ammonium oxalate (AOD) extraction than is ferrihydrite in the younger materials. Fe in the poorly crystalline smectite is subject to dissolution during citrate-bicarbonate-dithionite (CBD) extraction. The results indicate that relatively few mineralogical changes occur in these soils within the millennial time frame and under the environmental conditions associated with this study. Although the secondary mineral suite remains similar in the soils of different ages, ferrihydrite crystallinity appears to increase with increasing soil age.

Key Words—Fe mineralogy, Ferrihydrite, Smectite, Weathering, XAFS.

INTRODUCTION

Volcanic eruption products are important parent materials for soil formation in volcanically active regions of the world. Volcanic rocks and tephra are unstable under Earth-surface conditions and are often glassy, causing them to weather relatively rapidly, which releases dissolved Si, Al, Fe, and other elements. These elements re-precipitate in poorly crystalline phases including allophane, imogolite, ferrihydrite, and clay minerals (Fieldes, 1955; Shoji *et al.*, 1993). The distinctive soils formed by these processes are important in areas of the world where regular volcanic activity occurs, including New Zealand, Japan, Iceland, the Philippines, Indonesia, and the western Americas. The specific minerals formed depend on climate and on the mineralogy of the parent material, which can vary considerably depending on the type of volcanism occurring. Annual precipitation is an important factor because in wetter climates dissolved cations are removed from the weathering profile, whereas under drier conditions these cations accumulate in the soil, leading to the formation of aluminosilicates (Chadwick *et al.*, 2003). The typical mineral assemblage produced by the initial weathering of fresh basaltic parent rock includes allophane, ferrihydrite, and smectite clay minerals that are often ferruginous (Hay and Jones, 1972; Nahon *et al.*, 1982; Glasmann and Simonson, 1985; Eggleton *et al.*, 1987; Nesbitt and Young, 1989; Nesbitt and Wilson, 1992; Chorover *et al.*, 1999; Chadwick and Chorover, 2001; Chorover *et al.*, 2004; Rasmussen *et al.*, 2009). Characterization of minerals in soils developed on volcanic rocks and tephra is difficult because the minerals are often nano-sized and possess only short-range order, and thus are not easily detected using X-ray diffraction (XRD) (Hay and Jones, 1972; Colman, 1982b, 1982a).

Synchrotron-based X-ray absorption fine structure (XAFS) spectroscopic methods probe the immediate molecular environment around atoms, and are, therefore, useful in studying poorly crystalline materials. The near-edge region of the X-ray absorption spectrum (XANES) is sensitive to oxidation state and, in some cases, to molecular coordination and bonding of the target atom. The extended portion of the XAFS spectrum (EXAFS) probes the molecular environment immediately surrounding the target atom, yielding information on the identity and number of surrounding atoms and on their distances from the target atom. Thus, XAFS is particularly useful in the study of young weathering products, which are often characterized by a lack of long-range order.

Fe K-edge XANES and EXAFS spectra have been shown to be useful in distinguishing among the multitude of different Fe-bearing minerals (Manceau *et al.*, 1988, 1990; Dyar *et al.*, 2001, 2002; Wilke *et al.*, 2001, 2007; Gates *et al.*, 2002; Vantelon *et al.*, 2003; O'Day *et al.*, 2004; Prietzel *et al.*, 2007) and Fe-adsorbed phases (Karlsson *et al.*, 2008; Karlsson and Persson, 2009)

* E-mail address of corresponding author:
lbaker@uidaho.edu
†Current address: USDA-NRCS, Utah Snow Survey Office, Salt Lake City, UT 84116, USA
DOI: 10.1346/CCMN.2010.0580605

found in the environment. Many Fe-oxide minerals have distinctive XANES features. Some authors have argued, however, that XANES features are non-unique for some phases of similar chemistry and structure, particularly Fe (oxyhydr)oxides (Wilke *et al.*, 2001; O'Day *et al.*, 2004; Prietzel *et al.*, 2007). The EXAFS spectrum can often be used to distinguish among these phases, although the structures of poorly crystalline Fe (oxyhydr)oxides can vary continuously with composition, aging, and conditions rather than falling into easily distinguished groups (Schwertmann *et al.*, 2004; Toner *et al.*, 2009), complicating their spectroscopic identification.

XAFS spectroscopy can also be used to examine the speciation and distribution of Fe in a mineral structure where it substitutes isomorphically for another element. Significant Fe can be present in secondary phyllosilicates (Manceau *et al.*, 1990; Gualtieri *et al.*, 2000; Gates *et al.*, 2002; Vantelon *et al.*, 2003). The majority of Fe in phyllosilicates replaces Al in the octahedral sheet, but some Fe(III) may also replace Si in tetrahedral sites. Several studies have used EXAFS to investigate Fe distribution in suites of clay minerals. Gates *et al*. (2002) examined nontronites and ferruginous smectites using Fe-EXAFS and FTIR to quantify Fe distribution in octahedral and tetrahedral sites. Gualtieri *et al*. (2000) concluded from XANES spectra of kaolinites that substituted Fe was mostly in octahedral coordination, but some evidence suggested Fe might replace Si in tetrahedral coordination to a limited extent. Vantelon *et al*. (2003) examined Fe ordering in the octahedral sheet of montmorillonites and showed that XAFS could be used to distinguish different montmorillonites based on the extent of Fe-Fe next-neighbor pairing.

The present study examined a chronosquence of soils formed on basaltic cinders between 2 and 15 ka in age at Craters of the Moon National Monument (COM), Idaho, USA (Figure 1). This chronosequence was chosen in order to look at secondary mineral formation in andic soils on a millennial time scale under cool, dry conditions. Results from XANES, EXAFS, FTIR, XRD, electron microscopy, and selective extractions were used to examine the mineralogy of Fe in soil clays from the B horizons of the soils. The authigenic minerals in these soils do not possess long-range order and cannot be studied satisfactorily using conventional XRD analysis. Thus, XANES and EXAFS spectroscopy were used to provide insights into the Fe speciation and secondary mineralogy in the soil samples.

METHODS

Soil samples were collected from cinder cones at COM (Figure 1). The climate at the field site is cool and dry with an average annual precipitation of 393 mm and average maximum and minimum temperatures of 13 and −1ºC, respectively, although near-surface soil temperatures in summer can reach 65ºC on the dark basalt surfaces (Day and Wright, 1989). The majority of

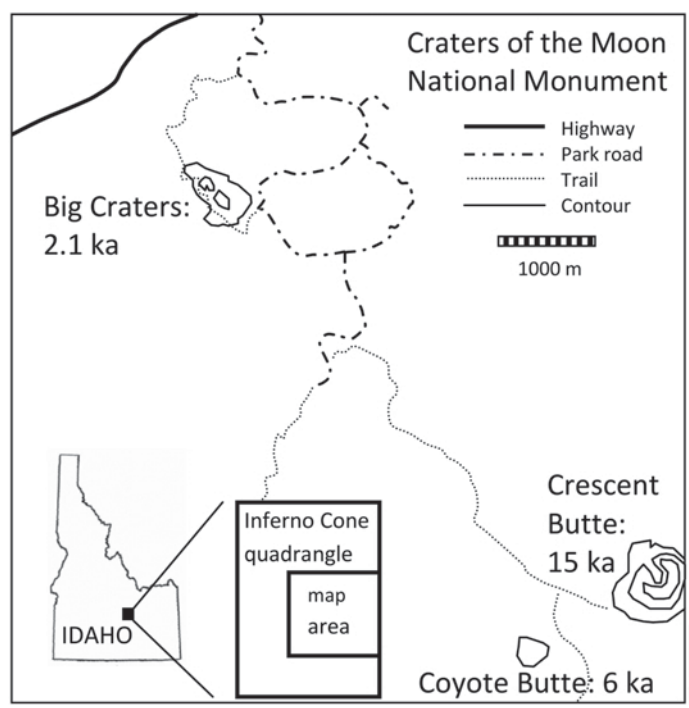

Figure 1. Location of sampling sites (Big Craters, Coyote Butte, and Crescent Butte), adapted from US Geological Survey 7.5 minute Inferno Cone quadrangle map (Kuntz *et al.*, 1989).

mapped soils in the area are classified as Andisols in terms of soil taxonomy (Soil Survey Staff, 2010). The soils were described and sampled using standard methods (Schoeneberger *et al.*, 2002; Soil Survey Staff, 2003) on soils formed in basaltic cinders at Big Craters, 2 ka; Coyote Butte, 6 ka; and Crescent Butte, 15 ka (Kuntz *et al.*, 1986, 1989) (Table 1, Figure 1). Samples from the B horizons were air dried and sieved to remove coarse (> 2 mm) fragments. Samples from the Bw1 and Bw2 horizons were collected separately at Coyote Butte and are referred to here as samples 6 ka(a) and 6 ka(b), respectively.

Texture analysis was carried out on the soil samples using sedimentation and sieving methods (Gee and Bauder, 1986). The clay (<0.002 mm) fractions from texture analysis were reserved, and splits of the clay fraction were extracted separately using ammonium oxalate in the dark (AOD) and citrate-bicarbonate-dithionite (CBD) (Jackson *et al.*, 1986). Samples of the unextracted clay fractions were sent for total chemical analysis to Acme Laboratories, Vancouver, British Columbia, Canada.

Unextracted and AOD-extracted soil samples were analyzed by XRD for bulk mineralogy on a Siemens D5000 diffractometer and the data were analyzed using the Bruker *Diffracplus Eva* evaluation program. The unextracted and AOD-extracted clay fractions were treated and analyzed for clay mineralogy by XRD (Whittig and Allardice, 1986; Harris and White, 2008). Both unextracted and AOD-extracted clay fractions were also analyzed by diffuse reflectance Fourier-transform infrared spectroscopy (FTIR) on a Perkin-Elmer System 2000, using a mixture of 3 wt.% clay in optical-grade KBr. Spectra were processed using the Kubelka-Munk algorithm provided in Perkin Elmer *Spectrum* 2.0 software. The AOD-extracted clays were examined by scanning electron microscopy (SEM) using an AMRAY 1830 with a Noran System Six electron dispersive spectroscopic analyzer (EDS) for semi-quantitative elemental analysis of individual particles.

Bulk Fe K-edge XAFS scans for unextracted and AOD-extracted soil clays and for all standards except allophane were collected on Beamline 10-2 of the Stanford Synchrotron Radiation Laboratory (SSRL). The monochromator for this beamline consisted of two parallel Si(220) crystals with a 6 mm entrance slit, and was detuned by 50% to minimize harmonics. All samples were run in a liquid He-cooled cryostat at a temperature of 6 K. Fluorescence data were collected using a 13-element Ge detector. Step size through the XANES region was 0.35 eV. The dry soil clays were packed into plastic sample holders and held in place with Kapton tape. X-ray absorption fine structure scans were also collected for laboratory-synthesized Fe-bearing standard minerals including goethite, two-line and six-line ferrihydrite, and allophane with 1 and 5 mol.% of Al replaced by Fe, and for commercially purchased hematite (JT Baker, Phillipsburg, New Jersey, USA), magnetite (DJ Minerals, Butte, Montana, USA), siderite (Wards, Rochester, New York, USA), pyrite (Wards), and beidellite SBId-1 (from the Source Clays Repository of The Clay Minerals Society). The standard mineral powders other than clay minerals were smeared on filter paper, which was cut into strips, stacked three layers thick, and sealed in the sample holder with Kapton tape. The beidellite clay standard was packed in a sample holder as for the soil clays. Fe-substituted allophane was synthesized using the method of Montarges-Pelletier *et al*. (2005). The allophane samples were packed into sample holders as for the soil clays and analyzed at the National Synchrotron Light Source (Brookhaven, New York, USA) on beamline X-11A at room temperature, using a double crystal Si(111) detuned by 30% to minimize harmonics. The fluorescence data were collected using a Lytle detector. Both transmission and fluorescence spectra were collected for all samples; fluorescence spectra were used when the quality of transmission spectra was poor. For samples in which both fluorescence and transmission data were of high quality, the two datasets were comparable and fluorescence data did not show any self-absorption artifacts.

One to six XAFS scans per sample were merged and calibrated using the program *SixPack* (Webb, 2005). Principal component analysis (PCA) and target transform (TT) to standards were carried out using k^3-weighted chi spectra in *SixPack* because these spectra contained more distinctive features than XANES spectra, and are less prone to intensity artifacts that affect XANES spectra as a result of small variations in sample thickness (Manceau and Gates, 1997). Target transform

Table 1. Percent clay from soil-particle size analysis, and the results of oxalate and dithionite extractions and total chemical analysis of the clay fraction.

Sample age	Depth (m)	% clay	Fe_{tot} (wt.%)	Fe_{dith} (wt.%)	Fe_{ox} (wt.%)
2 ka	0.07–0.18	7.8	12.7	11.6	11.4
6 ka (a)	0.16–0.24	5.8	12.4	12.4	10.9
6 ka (b)	0.24–0.31	6.8	14.0	13.3	12.4
15 ka	0.21–0.35	9.7	13.7	12.4	11.8

was used to test whether particular standard spectra were possible matches to components. The acceptability of a particular target as a possible component can be measured by the value of the SPOIL function (Malinowski, 1978, 1991). The SPOIL value is typically <3 for a good target, 3–6 for a moderately acceptable target, and >6 for an unacceptable target. Target transform was applied to the spectra of possible component clay minerals including beidellite, SBId-1, montmorillonite, SWy-2, illite, IMt-1, and nontronite, NAu-1, as well as to the Fe minerals hematite, magnetite, goethite, and siderite. Standards which had the smallest SPOIL values were used in the linear combination fitting (LCF) routine in *SixPack*. For PCA, TT, and LCF, the spectra were deglitched and windowed from k = 2.8 to 8.8 $Å^{-1}$ to reduce the effects of noise and crystal glitches on the fitting results. The number of significant components from PCA was evaluated based on the minimum value of the factor indicator function (IND) (Malinowski, 1991). Standard spectra used here were chosen for LCF on the basis of their SPOIL value, and included two-line ferrihydrite and beidellite. Additional LC fitting was also carried out using more than two components and standards with greater SPOIL values such as montmorillonite and allophane to determine whether inclusion of additional standards improved the fitting results.

RESULTS

Chemical and mineralogical analyses

Particle-size analysis showed that the four soil samples ranged from 5.8 to 9.7 wt.% clay (Table 1). Bulk chemical analysis indicated that the clay fraction contained 12.4–14.0 wt.% total Fe. For all four soil clays, CBD extracted 90–100% of total Fe, and AOD extracted 86–90% of total Fe (Table 1), suggesting that >86% of the Fe in the soil clays was present in poorly crystalline phases that are subject to dissolution by ammonium oxalate, with a relatively small proportion of total Fe in more crystalline mineral phases. Powder XRD analysis indicated that quartz and phyllosilicate minerals were the main crystalline phases present in the unextracted and AOD-extracted soil clays (Figure 2a). Crystalline Fe oxides such as hematite, goethite, and magnetite were not detected. X-ray diffraction scans of oriented Mg-saturated clay films from the AOD-extracted clay samples detected quartz, smectite, kaolinite, and illite. Evaluation of clay mineralogy in these samples by XRD proved difficult, requiring scan times of many hours to produce identifiable peaks (Figure 2b), suggesting that the clay minerals present were very poorly crystalline.

The FTIR spectra of unextracted soil clays (Figure 3) displayed broad peaks at 3400 cm^{-1} and 1040 cm^{-1}. The 3400 cm^{-1} peak resulted from hydroxyl stretching in hydrated amorphous materials such as ferrihydrite and allophane. The 1040 cm^{-1} peak resulted from Si–O stretching in silicate minerals, and in the non-AOD-extracted samples may be attributed to allophane, as indicated by its disappearance upon extraction. The absence of these features from the spectra of AOD-extracted samples confirms that amorphous oxides and silicates were, in fact, removed by the extraction. Removal of the spectral features due to hydrated amorphous materials revealed smaller IR peaks at 3695, 3620, 3200, 1090, 1040, 916, and 795 cm^{-1} in the spectra of the AOD-extracted samples. The peak at 3695 cm^{-1} is indicative of kaolinite, and the peaks at 3620 and 916 cm^{-1} are indicative of kaolinite, illite, and

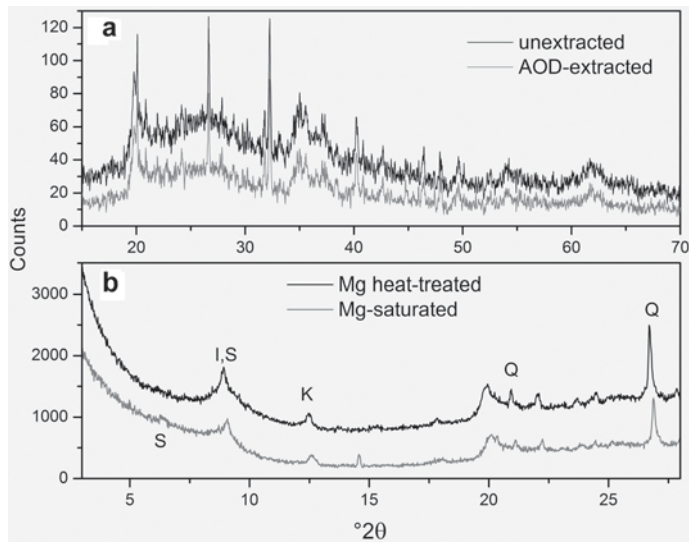

Figure 2. XRD patterns for powder-mounted, unextracted soil clay and AOD-extracted 15 ka soil clay (a), and for Mg-saturated AOD-extracted 15 ka soil clay and Mg-saturated clay heated overnight at 300ºC (b). Q: quartz; S: smectite; I: illite; K: kaolinite.

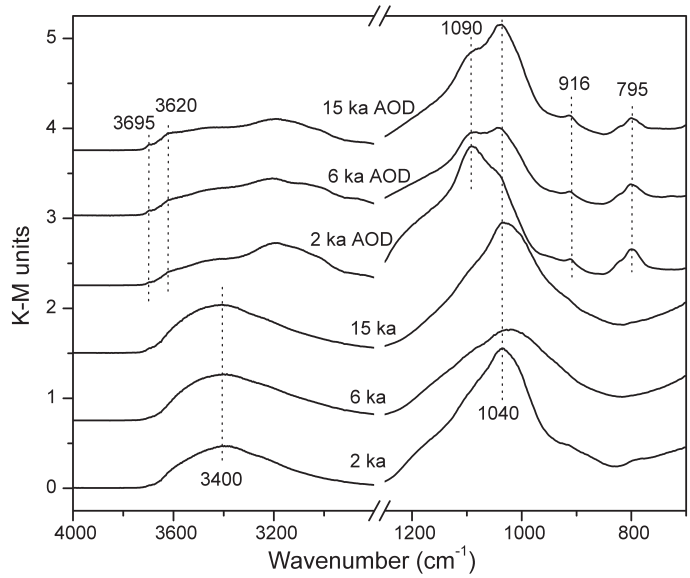

Figure 3. Diffuse reflectance FTIR spectra of unextracted and AOD-extracted soil clays. Dotted lines identify the peak positions. All spectra are plotted using the same vertical scale.

smectites, in agreement with the XRD analyses. The 795 cm^{-1} peak is indicative of quartz, the presence of which was also indicated by XRD analyses. The 1090 cm^{-1} peak is indicative of amorphous or opaline silica, which forms in ash-influenced soils as a weathering product of volcanic glass (Shoji *et al.*, 1993). Opaline silica, unlike allophane, is not removed by AOD treatment (Kodama and Wang, 1989), which explains the presence of this feature in the spectra of AOD-extracted samples. The prominence of this peak in younger samples suggests that opaline silica was more abundant in the youngest samples.

Analysis by SEM-EDS showed that all the AOD-extracted clays contained Fe-bearing aluminosilicate phases in the form of aggregates of μm-sized ovoid flakes (Figure 4), which may be clay minerals, and which had an aluminosilicate composition and contained detectable amounts of Fe and Ca (Figure 4, inset). The 15 ka AOD-extracted soil clay contained a few particles that were composed mostly of Fe and O. The particles were not observed in the younger soil clays, and may be relict ferrihydrite that was not dissolved during the AOD extraction, as discussed below. Aside from the presence of these particles in the 15 ka soil clay, all the AOD-extracted clays displayed similar morphology and elemental composition in the SEM analyses.

XANES and EXAFS analyses

The XANES spectra of unextracted soil clays most closely resemble the spectra of the two-line and six-line ferrihydrite standards, with a peak in the pre-edge region at 7110 eV and the main edge occuring at 7121 eV (Figure 5). The XANES spectra of crystalline (oxyhydr)-oxide minerals hematite, magnetite, or goethite and of Fe-substituted allophane had distinct features not present in the soil-clay XANES spectra. The XANES spectra of the AOD-extracted soil clays are most similar to the spectrum of the beidellite standard. The characteristic features of the beidellite first-derivative XANES spectrum include a pre-edge peak at 7113 eV, the main edge at 7122 eV, and a post-edge peak at 7130 eV. Peaks at these positions are also apparent in the spectra of the AOD-extracted soil clays, although they are less prominent in the 15 ka AOD-extracted sample, where the position of the edge peak at 7121 eV suggests that some ferrihydrite remained after AOD extraction.

Distinguishing between different Fe-substituted clay minerals is aided by analysis of the EXAFS chi spectra (Figure 6) and their Fourier transforms (Figure 7). The

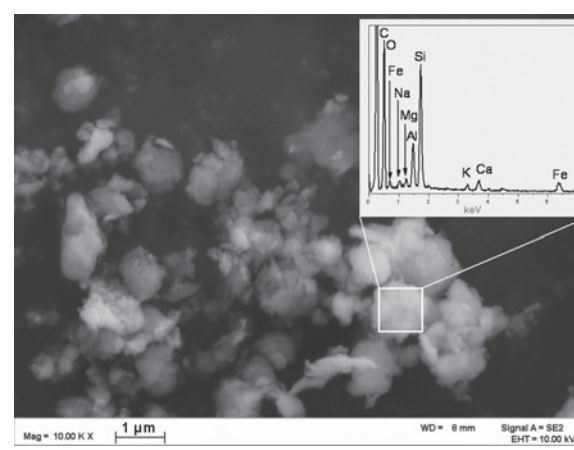

Figure 4. SEM image of an aluminosilicate aggregate in a 15 ka AOD-extracted sample, with an inset EDS graph of elemental composition of the particle indicated.

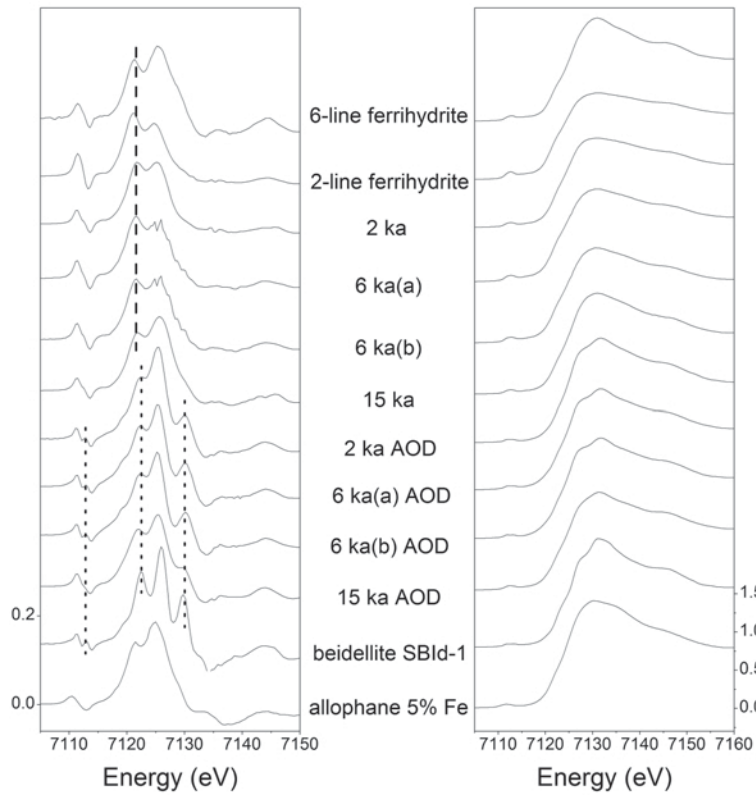

Figure 5. XANES and first-derivative XANES spectra of soil clays and standards. The dashed line shows the characteristic ferrihydrite edge position, and dotted lines show characteristic pre-edge, edge, and post-edge peak positions for clay minerals. All spectra are plotted using the same vertical scale, indicated at the bottom.

PCA of the chi spectra from all unextracted and extracted soil clay samples suggested that the eight spectra can be described by two end-member components. Target transform of the standard spectra showed that the most likely end members are two-line ferrihydrite (SPOIL = 4.27, chi squared = 14.8, R = 0.040) and beidellite SBId-1 (SPOIL = 5.84, chi squared = 91.1, R = 0.049). The six-line ferrihydrite standard is a moderately acceptable target (SPOIL = 5.75, chi squared = 55.2, R = 0.069), but less so than the two-line ferrihydrite. Similar results were obtained by carrying out PCA and target transform separately for the four unextracted and four AOD-extracted soil clays. As discussed above, target transform was carried out on the spectra of a large number of possible end-member mineral phases. No other spectra met the criteria for acceptable targets.

Based on the target transform, the two-line ferrihydrite and beidellite standards were identified as being the most probable end-member candidates for the soil clays, and were used for linear combination fitting of each of the soil clay spectra (Table 2). The Fe K-edge EXAFS spectra of montmorillonite and beidellite are very similar, suggesting that the EXAFS data may not be sensitive enough to distinguish between Fe-substituted beidellite and Fe-substituted smectite if the Fe content is small and Fe is distributed similarly in the octahedral sheet. Thus, the EXAFS data are interpreted here as indicating only that the Fe is present in an Fe-substituted dioctahedral smectite mineral. Montmorillonite and beidellite are common secondary phyllosilicates that weather from basaltic parent materials (Christidis, 2006), and so either is a reasonable candidate mineral in these soils.

The linear combination fitting (LCF) results indicated that Fe in the unextracted soil clays is present chiefly in ferrihydrite (Table 2). In the three younger AOD-extracted clays, LCF indicated that the smectite end-member is predominant. In the 15 ka AOD-extracted

Table 2. Percentage of Fe present in different mineral phases, from linear combination fitting of EXAFS spectra using beidellite (beid) and 2-line ferrihydrite (fh) as end-members.

Sample	Unextracted clay		AOD-extracted clay	
	% fh	% beid	% fh	% beid
2 ka	94	6	17	83
6 ka (a)	93	7	12	88
6 ka (b)	95	5	0	100
15 ka	93	7	80	20

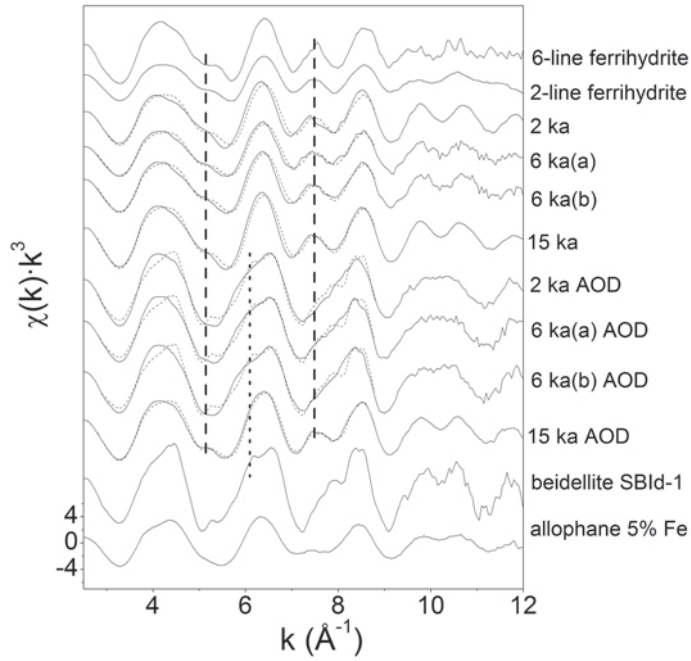

Figure 6. k^3-weighted chi spectra of soil clays and selected standards. Dotted curves show linear combination fits for k = 2.8−8.8 $Å^{-1}$. Distinctive spectral features of ferrihydrite are indicated by dashed lines and features of beidellite by dotted lines. All spectra are plotted using the same vertical scale, indicated at the bottom.

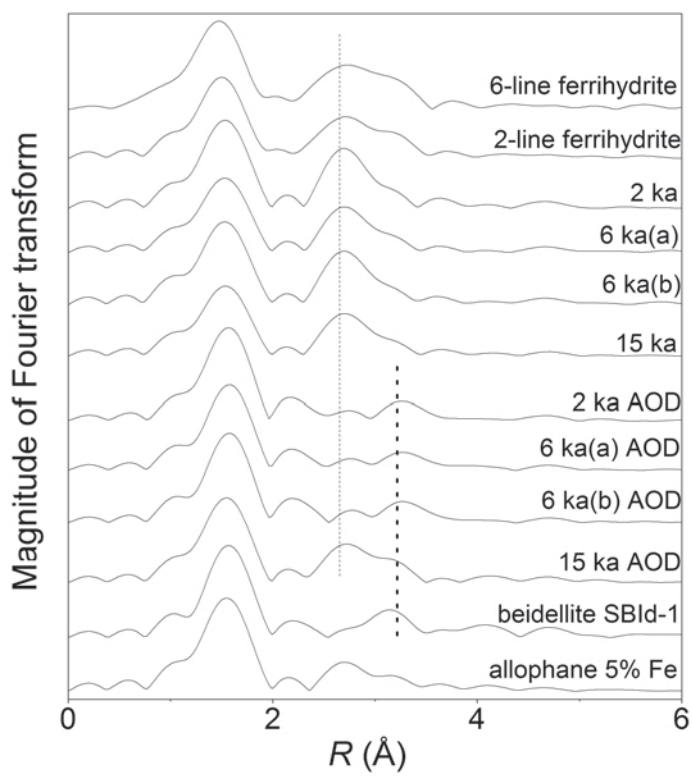

Figure 7. Magnitude of the Fourier-transformed XAFS data for soil clays, beidellite, and ferrihydrite standards. Dashed lines highlight distinctive shells for ferrihydrite and beidellite.

clay, the ferrihydrite component is the predominant contributor to the Fe XAFS spectrum (Table 2; Figures 5–7) although the smectite component is more abundant than in the non AOD-extracted 15 ka sample.

The LCF results (Table 2) indicate the mole percentage of Fe in the sample that is located in a particular end-member mineral, not the percentage of that mineral phase in the soil clay-size fraction. The LCF estimates of components in complex natural samples are typically considered to be subject to absolute detection limits of ~10%, and relative errors may approach ±25% (Ostergren *et al.*, 1999; Roberts *et al.*, 2002); however, for natural samples these percentages are difficult to quantify, especially for less-abundant species (Manceau *et al.*, 2000b). The standards used for LCF in this study include clay minerals containing substituted Fe, but the Fe contents of the standard clays may differ from the Fe contents of smectites in the soil clays. Furthermore, the Fe contents of soil clay smectites may vary among samples. Thus, the linear combination fit percentages shown in Table 2 should only be viewed as approximations of the amount of total Fe in the soil clay that is present in a ferrihydrite-like structure and in a smectite-like structure. A complete mass-balance calculation is not possible without independent information on the Fe content in the clay mineral.

DISCUSSION

The only detectable Fe-bearing phases present in any of the soil clays studied were ferrihydrite and a dioctahedral smectite containing isomorphically substituted Fe. This is consistent with most previous studies of weathering and soil development on basalts (Hay and Jones, 1972; Colman, 1982a, 1982b; Eggleton *et al.*, 1987; Nesbitt and Young, 1989; Nesbitt and Wilson, 1992) which found that the initial assemblage of secondary minerals typically includes poorly crystalline smectites, Fe (oxyhydr)oxides, and sometimes allophane. The presence of quartz in the clay-size samples suggests some eolian input to the soils because this mineral does not occur in basalts. Some of the clay minerals detected by XRD in the soil clays may also be eolian in origin. Wind-blown sediments are an important component of soils formed on basalts at COM (Vaughan, 2008). Sediments in the region, such as those deposited by the Big Lost River, are generally dominated by illite with some montmorillonite and minor kaolinite (Bartholomay *et al.*, 1989), so these minerals are present locally and could have been transported by wind to the sampling locations atop basaltic cinder cones. Another potential source of quartz and illite is silicic airfall tephra from rhyolite eruptions in the Snake River Plain, or from other regional silicic volcanism. The smectite detected in the soil clays by XRD and FTIR was probably authigenic because it is a typical product of early weathering of basalts. Smectite was also the only clay mineral in the soils that contained significant substituted Fe according to the XAFS data, suggesting that it formed in a different environment than the illite and kaolinite. Although the data do not unequivocally demonstrate that the smectite detected by XRD and FTIR is the same Fe-bearing smectite detected by XAFS, neither do the data indicate two separate smectite phases.

None of the standards tested was an excellent or good target based on the SPOIL factor value, and the linear combination fits do not perfectly reproduce every observable feature in the soil clay spectra, particularly for the AOD-extracted soil clays (Figure 6). This may be a result of the comparison of comparatively pure laboratory-synthesized or well crystallized natural minerals with poorly crystalline neoformed nanomineral phases in the soil. Several features, such as those at 4.6, 5.2, and 8.3 $Å^{-1}$, are more strongly developed in the LCF fits than in the soil clays. Fourier filtering of standard spectra and comparison with soil clay spectra (not shown) suggests that these features are mostly products of backscattering from more distant atomic shells in the beidellite standard. The poorly crystalline nature of the soil clay minerals may explain the absence of these features in the soil-clay spectra. This is less obvious in the ferrihydrite-dominated non-AOD extracted soil clays, perhaps because the ferrihydrite standards more closely approximate the poor crystallinity of the samples. The LCF results are clearly not perfect reproductions of the soil-clay spectra, but they were the highest-quality fits possible from a wide range of possible Fe-bearing end-members. Neither fitting with spectra from other Fe standard minerals nor using a larger number of standards in the fitting routine led to improvements in fitting results. A standard spectrum collected on a poorly crystalline Fe-substituted smectite might produce a better overall fit to the soil clay spectra, although the Fe-substituted allophane standard did not. The EXAFS results were supported by the XANES results, which indicated that significant Fe in the AOD-extracted soil clays was present in a smectitic clay mineral (Figure 5).

A typical interpretation of the selective extraction results shown in Table 1 would be that 86–90% of the total Fe in the soil clays is present as poorly crystalline oxides extractable by AOD, with up to 12% in crystalline Fe oxides extractable by CBD, and up to 10% of total Fe in another phase that was not affected by either of the extractants. The XRD and XAS results rule out the presence of significant crystalline Fe oxides, however, so the CBD-extractable Fe fraction must contain some other phase that is resistant to AOD but subject to attack by CBD. The Fe-substituted smectite is the only other Fe-bearing phase detected in the soil clays. The CBD extraction can remove some Fe from smectites. Typically CBD will reduce Fe(III) in clay minerals; however, most of the reduced Fe is retained in the structure of well crystallized clays rather than being completely dissolved (Roth *et al.*, 1969; Stucki *et al.*,

1984; Komadel *et al.*, 1995). The Fe in very small and poorly ordered clay minerals, such as those examined in the present study, may be more susceptible to CBD extraction. For example, in this study, LCF of the 6 ka(a) soil clay chi spectrum suggest that several percent of the total Fe in the unextracted sample was present in a smectite phase (Table 2, Figure 6), yet CBD extracted 100% of total Fe from this sample (Table 1).

The XAFS results are in agreement with the extraction data (Table 1), except for the 15 ka sample, in which ferrihydrite still dominated the XAFS spectrum after AOD extraction (Table 2; Figures 5, 6). Assuming that all the Fe remaining in the soil clay after extraction is in smectite, the Fe content of the smectite would be ~1.6−2.3 wt.%. Such an Fe content is not unusual for smectites, and the XAFS spectra measured in this study are similar to published spectra for montmorillonites of comparable Fe content with a small amount of Fe(III) isomorphically substituted for Al in the octahedral sheet and little or no Fe-Fe next-neighbor pairing (Vantelon *et al.*, 2003). Spectral features indicative of Fe-Fe next-neighbor pairing include a shoulder at k = 7.3 $Å^{-1}$ (Figure 6) and a peak at R = 2.6 Å in the Fourier transform (Figure 7) (Manceau *et al.*, 2000a; Gates *et al.*, 2002; Vantelon *et al.*, 2003). No such features were identified in the soil-clay spectra. The locations of these features are similar to Fe-Fe bonding features typical of ferrihydrite, and could thus confound the interpretation of EXAFS spectra, but distinguishing ferrihydrite from Fe-rich clay minerals is straightforward using the XANES spectra (Figure 5). Thus, the XAFS spectral features are consistent with the smectite Fe contents estimated from the extraction results.

Extraction with AOD removed 83−100% of the ferrihydrite Fe-EXAFS signal from the 2 ka and 6 ka soil clays according to LCF (Table 2), whereas the AOD-extracted 15 ka spectrum was still strongly dominated by the ferrihydrite component (Table 2; Figures 5, 6), suggesting that AOD-resistant ferrihydrite was present in the 15 ka sample, although the amount must be small because 86% of total Fe in the sample was extracted by AOD. As discussed above, SEM analysis of the 15 ka sample revealed the presence of sparse, mm-sized grains composed of Fe and O. These particles may be grains of ferrihydrite which were not extracted by AOD. Additionally, the extracted 15 ka clay sample had a redder hue than the younger soil clays, which were gray after AOD extraction, supporting the XAFS data interpretation that ferrihydrite persisted in the sample.

The AOD-resistant ferrihydrite in the oldest sample may be more crystalline than ferrihydrite in the younger samples. Samples of ferrihydrite exhibiting different degrees of crystallinity have been shown to exhibit different dissolution rates (Schwertmann *et al.*, 1982; Dold, 2003). The soil clay samples in this study were all extracted for 4 h, and variations in ferrihydrite crystallinity in the samples may have led to differences in the proportion of ferrihydrite extracted during this time. Extrapolation of ferrihydrite dissolution data presented by Dold (2003) suggests that a 4 h extraction would remove 100% of 2-line ferrihydrite, but only ~50% of 6-line ferrihydrite. However, the observation that a 4 h AOD extraction removed 86% of Fe from the 15 ka soil clay indicates that most ferrihydrite in this sample was easily extracted and that the proportion of more crystalline ferrihydrite present in the sample must have been small.

The structure and ordering of ferrihydrite has been the topic of considerable study. Ferrihydrites are typically identified by XRD as being of either 2-line or 6-line types and these two forms may result from differing conditions of formation or differences in crystallization kinetics (Schwertmann *et al.*, 1999). However, experiments that varied ferrihydrite synthesis conditions incrementally showed that a continuous series of structures can be produced ranging from 2-line ferrihydrite through intermediate types to 6-line ferrihydrite and on to hematite (Schwertmann *et al.*, 2004). The currently accepted structural model suggests that the ferrihydrite structure is composed of a mixture of three domain types, including defective crystallites, defect-free crystallites, and dispersed crystallites of hematite (Drits *et al.*, 1993; Manceau, 2009), with the more structured 6-line ferrihydrite containing domains of larger size than the 2-line form. This concept presumably allows for intermediate forms of ferrihydrite having intermediate domain sizes.

The EXAFS spectrum of ferrihydrite contains features typical of Fe in octahedral coordination, where neighboring octahedra display both corner-sharing and edge-sharing Fe-O linkages (Manceau and Drits, 1993; Toner *et al.*, 2009). The spectrum of more crystalline 6-line ferrihydrite has a greater amplitude than that of 2-line ferrihydrite (Manceau, 2009). It also displays more extensive development of the characteristic spectral features at k = 5.1 and 7.3 $Å^{-1}$, which indicates the increasing development of corner-sharing linkages in the structure (Toner *et al.*, 2009). The EXAFS spectral features may be used as indicators of the relative degree of crystallinity of a ferrihydrite sample. The soil clays examined in this study have greater EXAFS amplitudes than the 2-line ferrihydrite standard, but are otherwise more similar to 2-line than to 6-line ferrihydrite. The features at k = 5.1 and 7.3 $Å^{-1}$ are more strongly developed in the 15 ka soil clay, particularly after AOD extraction, but are still not as well developed as in the 6-line ferrihydrite sample (Figure 6). Thus, the data suggest that the ferrihydrite in all the soil clays is the 2-line type, but the 15 ka sample contains a small amount of somewhat more crystalline ferrihydrite.

CONCLUSIONS

X-ray absorption spectroscopy was used in combination with XRD, FTIR, and selective extractions to

characterize the mineralogy of Fe in a chronosequence of soil clays formed in basaltic cinders under cool, dry conditions. Over 90% of the Fe present in the soil clays is contained in ferrihydrite, with the remainder in an Fe-substituted smectitic clay mineral. The small amount of Fe in smectite can be detected in the soil clays by LCF of XAFS spectra, and this detection is confirmed by XAFS of AOD-extracted samples. The smectite is estimated to contain up to 2.3 wt.% Fe, some of which is extractable using CBD. The soil clays collected from older basalts contain ferrihydrite that is more resistant to extraction with AOD, suggesting an increase in crystallinity with sample aging.

ACKNOWLEDGMENTS

The authors thank Dr Andreas Voegelin for sharing EXAFS spectra, and the research group of D.L. Sparks for collecting XAFS data for allophane. Anita Falen provided invaluable assistance with soil extractions. Portions of this research were carried out at the Stanford Synchrotron Radiation Lightsource, a national user facility operated by Stanford University on behalf of the U.S. Department of Energy, Office of Basic Energy Sciences. The SSRL Structural Molecular Biology Program is supported by the Department of Energy, Office of Biological and Environmental Research, and by the National Institutes of Health, National Center for Research Resources, Biomedical Technology Program. The constructive comments of two referees are greatly appreciated.

REFERENCES

Bartholomay, R.C., Knobel, L.L., and Davis, L.C. (1989) *Mineralogy and grain size of surficial sediment from the Big Lost River drainage and vicinity, with chemical and physical characteristics of geologic materials from selected sites at the Idaho National Engineering Laboratory, Idaho*. USGS Open File Report 89−384. U.S. Geological Survey, Idaho Falls, Idaho, USA.

Chadwick, O.A. and Chorover, J. (2001) The chemistry of pedogenic thresholds. *Geoderma* **100**, 321−353.

Chadwick, O.A., Gavenda, R.T., Kelly, E.F., Ziegler, K., Olson, C.G., Elliott, W.C., and Hendricks, D.M. (2003) The impact of climate on the biogeochemical functioning of volcanic soils. *Chemical Geology*, **202**, 195−223.

Chorover, J., DiChiaro, M.J., and Chadwick, O.A. (1999) Structural charge and cesium retention in a chronosequence of tephritic soils. *Soil Science Society of America Journal*, **63**,169−177.

Chorover, J., Amistadi, M.K., and Chadwick, O.A. (2004) Surface charge evolution of mineral-organic complexes during pedogenesis in Hawaiian basalt. *Geochimica et Cosmochimica Acta*, **68**, 4859−4876.

Christidis, G.E. (2006) Genesis and compositional heterogeneity of smectites. Part III: Alteration of basic pyroclastic rocks − A case study from the Troodos Ophiolite Complex, Cyprus. *American Mineralogist*, **91**, 685−701.

Colman, S.M. (1982a) Clay mineralogy of weathering rinds and possible implications concerning the sources of clay minerals in soils. *Geology*, **10**, 370−375.

Colman, S.M. (1982b) *Chemical Weathering of Basalts and Andesites: Evidence from Weathering Rinds*. U.S. Geological Survey Professional Paper **1246**. Government Printing Office, Washington, D.C.

Day, T.A. and Wright, R.G. (1989) Positive plant spatial association with *Eriogonum ovalifolium* in primary succession on cinder cones: seed-trapping nurse plants. *Plant Ecology*, **80**, 37−45.

Dold, B. (2003) Dissolution kinetics of schwertmannite and ferrihydrite in oxidized mine samples and their detection by differential X-ray diffraction (DXRD). *Applied Geochemistry*, **18**, 1531−1540.

Drits, V.A., Sakharov, B.A., Salyn, A.L., and Manceau, A. (1993) Structural model for ferrihydrite. *Clay Minerals*, **28**, 185−207.

Dyar, M.D., Delaney, J.S., and Sutton, S.R. (2001) Fe XANES spectra of iron-rich micas. *European Journal of Mineralogy*, **13**, 1079−1098.

Dyar, M.D., Lowe, E.W., Guidotti, C.V., and Delaney, J.S. (2002) Fe^{3+} and Fe^{2+} partitioning among silicates in metapelites: A synchrotron micro-XANES study. *American Mineralogist*, **87**, 514−522.

Eggleton, R.A., Foudoulis, C., and Varkevisser, D. (1987) Weathering of basalt; changes in rock chemistry and mineralogy. *Clays and Clay Minerals*, **35**, 161−169.

Fieldes, M. (1955) Clay mineralogy of New Zealand soils, Part II: Allophane and related mineral colloids. *New Zealand Journal of Science and Technology*, **B37**, 336−350.

Gates, W.P., Slade, P.G., Manceau, A., and Lanson, B. (2002) Site occupancies by iron in nontronites. *Clays and Clay Minerals*, **50**, 223−239.

Gee, G.W. and Bauder, J.W. (1986) Particle-size analysis. Pp. 383−441 in: *Methods of Soil Analysis. Part 1* (A. Klute, editor). Soil Science Society of America and American Society of Agronomy, Madison, Wisconsin, USA.

Glasmann, J.R. and Simonson, G.H. (1985) Alteration of basalt in soils of western Oregon. *Soil Science Society of America Journal*, **49**, 262−273.

Gualtieri, A.F., Moen, A., and Nicholson, D.G. (2000) XANES study of the local environment of iron in natural kaolinites. *European Journal of Mineralogy*, **12**, 17−23.

Harris, W. and White, G.N. (2008) X-ray diffraction techniques for soil mineral identification. Pp. 81−115 in: *Methods of Soil Analysis. Part 5. Mineralogical Methods* (A.L. Ulery and L.R. Drees, editors). Soil Science Society of America, Madison, Wisconsin, USA.

Hay, R.L. and Jones, B.F. (1972) Weathering of basaltic tephra on the island of Hawaii. *Geological Society of America Bulletin*, **83**, 317−332.

Jackson, M.L., Lim, C.H., and Zelazny, L.W. (1986) Oxides, hydroxides, and aluminosilicates. Pp. 101−142 in: *Methods of Soil Analysis*, Vol. **1**, 2nd edition (A. Klute, editor). Soil Science Society of America, Madison, Wisconsin, USA.

Karlsson, T. and Persson, P. (2009) Coordination chemistry and hydrolysis of Fe(III) in a peat humic acid studied by X-ray absorption spectroscopy. *Geochimica et Cosmochimica Acta*, **74**, 30−40.

Karlsson, T., Persson, P., Skyllberg, U., Mörth, C.-M., and Giesler, R. (2008) Characterization of iron(III) in organic soils using extended x-ray absorption fine structure spectroscopy. *Environmental Science and Technology*, **42**, 5449−5454.

Kodama, H. and Wang, C. (1989) Distribution and characterization of noncrystalline inorganic components in spodosols and spodosol-like soils. *Soil Science Society of America Journal*, **53**, 526−534.

Komadel, P., Madejová, J., and Stucki, J.W. (1995) Reduction and reoxidation of nontronite: Questions of reversibility. *Clays and Clay Minerals*, **43**, 105−110.

Kuntz, M.A., Champion, D.E., Spiker, E.C., and Lefebvre, R.H. (1986) Contrasting magma types and steady-state, volume-predictable, basaltic volcanism along the Great Rift, Idaho. *Geological Society of America Bulletin*, **97**, 579−594.

Kuntz, M.A., Champion, D.E., Lefebvre, R.H., and Covington, H.R. (1989) *Geologic Map of the Inferno Cone Quadrangle, Butte County, Idaho*. U.S. Geological Survey Geologic Quadrangle Map GQ-1632, USA.

Malinowski, E.R. (1978) Theory of error for target factor analysis with applications to mass spectrometry and nuclear magnetic resonance spectrometry. *Analytica Chimica Acta*, **103**, 339–354.

Malinowski, E.R. (1991) *Factor Analysis in Chemistry*, 2nd edition. Wiley, New York.

Manceau, A. (2009) Evaluation of the structural model for ferrihydrite derived from real-space modelling of high-energy X-ray diffraction data. *Clay Minerals*, **44**, 19–34.

Manceau, A. and Drits, V.A. (1993) Local structure of ferrihydrite and feroxyhite by EXAFS spectroscopy. *Clay Minerals*, **28**, 165–184.

Manceau, A. and Gates, W.P. (1997) Surface structural model for ferrihydrite. *Clays and Clay Minerals*, **45**, 448–460.

Manceau, A., Bonnin, D., Kaiser, P., and Frétigny, C. (1988) Polarized EXAFS of biotite and chlorite. *Physics and Chemistry of Minerals*, **16**, 180–185.

Manceau, A., Bonnin, D., Stone, W.E.E., and Sanz, J. (1990) Distribution of Fe in the octahedral sheet of trioctahedral micas by polarized EXAFS; comparison with NMR results. *Physics and Chemistry of Minerals*, **17**, 363–370.

Manceau, A., Lanson, B., Drits, V.A., Chateigner, D., Gates, W.P., Wu, J., Huo, D., and Stucki, J.W. (2000a) Oxidation-reduction mechanism of iron in dioctahedral smectites: I. Crystal chemistry of oxidized reference nontronites. *American Mineralogist*, **85**, 133–152.

Manceau, A., Lanson, B., Schlegel, M.L., Harge, J.C., Musso, M., Eybert-Berard, L., Hazemann, J.-L., Chateigner, D., and Lamble, G.M. (2000b) Quantitative Zn speciation in smelter-contaminated soils by EXAFS spectroscopy. *American Journal of Science*, **300**, 289–343.

Montarges-Pelletier, E., Bogenez, S., Pelletier, M., Razafitianamaharavo, A., Ghanbaja, J., Lartiges, B., and Michot, L. (2005) Synthetic allophane-like particles: textural properties. *Colloids and Surfaces A: Physicochemical and Engineering Aspects*, **255**, 1–10.

Nahon, D., Colin, F., and Tardy, Y. (1982) Formation and distribution of Mg, Fe, Mn-smectites in the first stages of the lateritic weathering of forsterite and tephroite. *Clay Minerals*, **17**, 339–348.

Nesbitt, H.W. and Young, G.M. (1989) Formation and diagenesis of weathering profiles. *Journal of Geology*, **97**, 129–147.

Nesbitt, H.W. and Wilson, R.E. (1992) Recent chemical weathering of basalts. *American Journal of Science*, **292**, 740–777.

O'Day, P.A., Rivera, N., Root, R., and Carroll, S.A. (2004) X-ray absorption spectroscopic study of Fe reference compounds for the analysis of natural sediments. *American Mineralogist*, **89**, 572–585.

Ostergren, J.D., Brown, G.E., Parks, G.A., and Tingle, T.N. (1999) Quantitative speciation of lead in selected mine tailings from Leadville, CO. *Environmental Science and Technology*, **33**, 1627–1636.

Prietzel, J., Thieme, J., Eusterhues, K., and Eichert, D. (2007) Iron speciation in soils and soil aggregates by synchrotron-based X-ray microspectroscopy (XANES, m-XANES). *European Journal of Soil Science*, **58**, 1027–1041.

Rasmussen, C., Dahlgren, R.A., and Southard, R.J. (2009) Basalt weathering and pedogenesis across an environmental gradient in the southern Cascade Range, California, USA. *Geoderma*, **154**, 473–485.

Roberts, D.R., Scheinost, A.C., and Sparks, D.L. (2002) Zinc speciation in a smelter-contaminated soil profile using bulk and microspectroscopic techniques. *Environmental Science and Technology*, **36**, 1742–1750.

Roth, C.B., Jackson, M.L., and Syers, J.K. (1969) Deferration effect on structural ferrous-ferric iron ratio and CEC of vermiculites and soils. *Clays and Clay Minerals*, **17**, 253–264.

Schoeneberger, P.J., Wysocki, D.A., Benham, E.C., and Broderson, W.D., (editors) (2002) *Field Book for Describing and Sampling Soils, Version 2*. Natural Resources Conservation Service, Lincoln, Nebraska, USA.

Schwertmann, U., Schulze, D.G., and Murad, E. (1982) Identification of ferrihydrite in soils by dissolution kinetics, differential X-ray diffraction, and Mössbauer spectroscopy. *Soil Science Society of America Journal*, **46**, 869–875.

Schwertmann, U., Friedl, J., and Stanjek, H. (1999) From Fe(III) ions to ferrihydrite and then to hematite. *Journal of Colloid and Interface Science*, **209**, 215–223.

Schwertmann, U., Friedl, J., and Kyek, A. (2004) Formation and properties of a continuous crystallinity series of synthetic ferrihydrites (2- to 6-line) and their relation to FeOOH forms. *Clays and Clay Minerals*, **52**, 221–226.

Shoji, S., Nanzyo, M., and Dahlgren, R. (1993) *Volcanic Ash Soils: Genesis, Properties and Utilization.* Elsevier, New York.

Soil Survey Staff (2003) *Keys to Soil Taxonomy*, 9th edition. US Government Printing Office, Washington, D.C.

Soil Survey Staff (2010) *Web Soil Survey*. US Department of Agriculture – Natural Resources Conservation Service, USA.

Stucki, J.W., Golden, D.C., and Roth, C.B. (1984) Effects of reduction and reoxidation of structural iron on the surface charge and dissolution of dioctahedral smectites. *Clays and Clay Minerals*, **32**, 350–356.

Toner, B.M., Santelli, C.M., Marcus, M.A., Wirth, R., Chan, C.S., McCollom, T., Bach, W., and Edwards, K.J. (2009) Biogenic iron oxyhydroxide formation at mid-ocean ridge hydrothermal vents: Juan de Fuca Ridge. *Geochimica et Cosmochimica Acta*, **73**, 388–403.

Vantelon, D., Montarges-Pelletier, E., Michot, L.J., Pelletier, M., Thomas, F., and Briois, V. (2003) Iron distribution in the octahedral sheet of dioctahedral smectites. An Fe K-edge X-ray absorption spectroscopy study. *Physics and Chemistry of Minerals*, **30**, 44–53.

Vaughan, K.L. (2008) Pedogenesis at Craters of the Moon National Monument and Preserve, Idaho, USA. PhD dissertation, University of Idaho, Moscow, Idaho, USA.

Webb, S.M. (2005) *Sixpack*: A graphical user interface for XAS analysis using IFEFFIT. *Physica Scripta*, **T115**, 1011–1014.

Whittig, L.D. and Allardice, W.R. (1986) X-ray diffraction techniques. P. 1188 in: *Methods of Soil Analysis – Part 1: Physical and Mineralogical Methods*, Vol. **1**, 2nd edition (A. Klute, editor). Soil Science Society of America, Madison, Wisconsin, USA.

Wilke, M., Farges, F., Petit, P.-E., Brown, G.E., Jr., and Martin, F. (2001) Oxidation state and coordination of Fe in minerals: An Fe K-XANES spectroscopic study. *American Mineralogist*, **86**, 714–730.

Wilke, M., Farges, F., Partzsch, G.M., Schmidt, C., and Behrens, H. (2007) Speciation of Fe in silicate glasses and melts by in-situ XANES spectroscopy. *American Mineralogist*, **92**, 44–56.

(*Received 29 April 2010; revised 29 October 2010; Ms. 435; AE: B. Lanson*)